NUMERICAL VS ANALYTICAL COMPARISON WITH EXPERIMENTAL FFR VALUES OF RIGHT CORONARY ARTERY STENOSIS

Aleksandar Milovanovic[a]*, Igor Saveljic[a,c], Nenad Filipovic[b,c]

[a]Institute for information technologies, University of Kragujevac, 34000 Kragujevac, Serbia

[b]Faculty of Engineering, University of Kragujevac, 34000 Kragujevac, Serbia

[c]Bioengineering Research and Development Center, 34000 Kragujevac, Serbia

*Corresponding author: Aleksandar Milovanovic, Institute for information technologies,

University of Kragujevac, 34000 Kragujevac, Serbia. E-mail: acakg85@hotmail.com

Abstract.

BACKGROUND: Fractional flow reserve (FFR) index has been widely accepted as a standard diagnostic method for identifying functional relevance of coronary stenosis. Since the invasive techniques used for its determination are associated with a certain risk of vascular injury, as well as with an increased cost, the several non-invasive procedures have been developed.

OBJECTIVE: The aim of this study was to compare FFR values for the coronary artery obtained by Computational Fluid Dynamics (CFD) and Coronary Computed Tomography Angiography (CCTA).

METHODS: Computation of FFR has been performed using both the numerical method and the analytical method. The numerical method employs CFD to solve the governing equations which relate to mass and momentum conservation (the continuity equation and the Navier-Stokes equations) as well as CCTA to generate the three-dimensional computational domain. After imposing the appropriate boundary conditions the values of the pressure change are calculated and the FFR index is determined. Based on Bernoulli's law, the analytical

method calculates the overall pressure drop across the stenosis in the coronary artery, enabling FFR determination.

RESULTS: The clinical data for twenty patients who underwent invasive coronary angiography are used to validate the results obtained by using CFD (together with CCTA) simulation and analytical solution. The medically measured FFR compared to the analytical one differs by about 4%, while, when compared to the numerical FFR, the difference is about 2.6%. For FFR values below 0.8 (which are considered to be associated with myocardial ischemia) the standard error has a value of 0.01201, while the standard deviation is 0.02081. For FFR values above 0.80, these values are slightly higher. Bland-Altman analysis has been shown that medical measurement and numerical FFR was in good agreement (SD=0.0292, p<0.0001).

CONCLUSIONS: The analytically calculated FFR has a slightly lower coefficient of determination than numerically computed when compared with experimental one. However, it still can give a reliable answer to the question of whether patients need a stent, bypass surgery or only drug treatment and it requires a significantly lower computation time.

Keywords: Coronary artery stenosis, fractional flow reserve, CFD, Bernoulli's law.

1. Introduction

The coronary artery disease (CAD) is the most prevalent heart disease throughout the world today. It is caused by atherosclerosis and affects the blood vessels (arteries) that feed the heart with blood and oxygen. This disease occurs when the coronary arteries narrow or become blocked by cholesterol plaque formation. As plaque builds up the blood vessel wall becomes thicker (Fig. 1), at the same time reducing or even blocking blood flow to the heart muscle. Myocardial ischemia can cause chest discomfort (angina pectoris) and, if plaques rupture or

bursts, may result in myocardial infarction (heart attack) [1-2]. According to the World Health Organization in 2019 there were globally 17.9 million deaths caused by cardiovascular diseases, accounting for 32.84 % of all deaths. It is considerably higher than cancer, the second leading cause of death (17.83 %).

Figure 1. Coronary artery disease [2]

The existence of myocardial ischemia is the predominant risk factor significantly related to adverse clinical outcome. Therefore, an early diagnosis and treatment of CAD is of paramount importance because it can prevent the development of complications [3]. Timely revascularisation of coronary artery stenosis that induces myocardial ischemia offers notable improvement of patient outcomes.

There are few diagnostic methods, both invasive and non-invasive. The standard invasive method, an invasive coronary angiography (ICA), is very reliable in determining location and severity of stenosis. It uses x-rays to make pictures of patient's blood vessels [4]. In order to make the vessels to be visible it requires injection of a liquid dye through a long tiny tube (catheter) into the coronary artery. This dye enables the blood inside artery to be visible on an x-ray and, thus, detection of the blockage (stenosis) that may exist in blood vessels. Although the visual assessment of stenosis provides information regarding its severity still the coronary angiography cannot fully define the functional significance of stenosis. Therefore, the decisions regarding CAD treatment (medical therapy, percutaneous coronary interventions, or surgical revascularization) based on invasive coronary angiography is not fully reliable. It has been reported [5] that ICA can underestimate or overestimate stenosis severity, particularly in case of moderate stenosis. That is because not only the blood vessel narrowing but also several other factors, including the length of stenosis, its shape, and location, the existence of collateral flow or the amount of viable myocardium also

contribute to ischemia. It means that the same degree of stenosis may have different influence to different patients. Generally, the invasive coronary angiography can be both diagnostic and therapeutic.

Since the invasive techniques are connected with a certain risk of vascular injury [6], as well as with an additional cost, it was prudent to develop an affective non-invasive methods both to ensure reliable diagnose and protect patients from undesirable consequences. Non-invasive diagnostic methods are mostly based on computerized tomography. A computed tomography (CT) coronary angiography has been established as a non-invasive and low cost diagnostic tool for identifying coronary stenosis severity [7]. Although CT coronary angiography has proven an accurate detection of coronary stenosis, a number of studies [8-10] have reported its unreliable relationship to lesion-specific ischemia with false positive rate when compared with invasive coronary angiography. Furthermore, this technique also is not able to evaluate the hemodynamic significance of coronary lesions [11].

In contrast, it has been proven by numerous researches [12-14] that a Fractional Flow Reserve (FFR) index obtained by Invasive Coronary Angiography (ICA) has become the standard method for evaluating the anatomical and physiological significance of coronary artery stenosis, and, therefore, as a decisive parameter for revascularization therapy. Tonino et al. [15] proved the clinical benefit of FFR-guided interventions on outcome of patients. However, in recent years an enhanced potential of FFR acquired from coronary CT angiography has been proven by applying an advanced computational fluid dynamic modelling [4, 16]. It allows the possibility of improving the outcomes while reducing the costs.

1.1 Fractional flow reserve (FFR)

Fractional flow reserve (FFR) initially proposed and verified in a landmark study by Pijls et al. [17] in 1996, represents a ratio of the maximum myocardial flow rate through the supplying coronary artery with stenosis to the maximum flow rate through the hypothetically normal artery. Therefore, an angiographic based FFR, according to [17] is defined as:

$$FFR_Q = \frac{Q_S}{Q_N}, \tag{1}$$

where Q_S is myocardial flow rate through stenotic artery, while Q_N is myocardial flow through hypothetically normal artery defined as [18]:

$$Q_S = \frac{P_d - P_v}{R_{min\,S}} \quad \text{and} \quad Q_N = \frac{P_a - P_v}{R_{min\,N}}, \tag{2}$$

where $R_{min\,S}$ and $R_{min\,N}$ are minimal resistances for the distal microcirculation with and without stenosis in the coronary artery (Fig. 2), while P_d is the arterial pressure distal to the stenosis, P_a is proximal arterial pressure (equal to aortic pressure) and P_v is coronary venous pressure.

Figure 2. Model of the coronary circulation

By substituting equations (2) into equation (1) we obtain:

$$FFR_Q = \frac{Q_S}{Q_N} = \frac{P_d - P_v}{P_a - P_v} \frac{R_{min\,N}}{R_{min\,S}}. \tag{3}$$

FFR based on pressure is defined as:

$$FFR_P = \frac{P_d - P_v}{P_a - P_v}. \tag{4}$$

During maximal hyperemia minimal resistance for the distal microcirculation does not depend on hemodynamic conditions and epicardial stenosis, thus $R_{min\,S} = R_{min\,N}$ [18]. In that case equation (3) takes the form (4), i.e. FFR$_Q$ becomes equal to FFR$_P$:

$$FFR_P = FFR_Q = \frac{P_d - P_v}{P_a - P_v} \,.$$
(5)

The aortic (proximal), distal and coronary venous pressures can easily be measured during coronary angiography using a pressure probe.

FFR in a normal coronary artery has a value of 1.0, regardless of the patient. The values above 0.80 are usually not associated with ischemia, while stenosis with FFR ≤ 0.75 indicates severe stenosis with a remarkably high accuracy, and therefore, a high demand for revascularization [19].

In order to check the above assumption and validity of equation (5) Pijls et al [17] compared pressure based FFR (4) with the angiographic based flow ratio Q_S/Q_N (1). They found out that with an increase of stenosis severity the pressure-based FFR progressively underestimates the FFR from myocardial flow ratio. The possibility of using angiographic image data to measure coronary flow rate was verified by using flow probe [20]. Wong et al. [21] reported a linear correlation between the angiographic FFR and the clinical pressure-wire based FFR and concluded that computation of FFR by using angiographic images has been proved to be an efficient tool in assessing a severity of stenosis [22].

Currently, the clinical measurement of FFR is pressure based (FFR$_P$) which uses the approximation of equation (5) [23]:

$$FFR_p = \frac{P_d}{P_a} = \frac{P_a - \Delta P}{P_a} \,.$$
(6)

where ΔP is the pressure drop across stenosis.

The aim of this study is to validate the analytical and numerical algorithms for computation of FFR from CCTA data by comparing them with the invasively measured ones.

2. A literature review of analytical and numerical solutions to the Fractional Flow Reserve (FFR)

Although FFR obtained by measuring the pressure difference across stenosis using pressure wire is considered as a standard for assessing hemodynamic significance of artery stenosis there are few shortcomings such as a potential risk for patients, the costs of the pressure wire, and disturbance of blood flow induced by the wire. Also, it requires an injection of adenosine in order to induce maximal hyperemia. In order to overcome these shortcomings the development of non-invasive methods was initiated.

The advances made in the area of computational fluid dynamics (CFD) and image-based modelling enable determination of coronary flow and pressure field. Taylor et all [24] were first to propose non-invasive calculation of FFR by using a computerized numerical simulation. It has been proved that CFD together with CCTA [25] can accurately identify and assess coronary lesions that cause ischemia. As a result of coronary flow simulation using CFD technique non-invasive Fractional Flow Reserve (FFR_{CT}) can be derived without additional medical interventions [26].

The accuracy of blood flow simulation by applying CFD depends on many factors such as the quality of geometry reconstruction, mesh quality, the used numerical method and appropriate boundary conditions. FFR_{CT} computation is usually performed using the following assumptions [27]:

(1) At rest, the artery supply is in proportion to the myocardial oxygen need;

(2) Resistance of the microcirculation is in inverse proportion to the size of the coronary artery;

(3) Coronary microcirculation has a predictable response to maximal hyperaemic conditions.

Despite its complex rheology blood can be considered as an incompressible Newtonian fluid when considering flow through large arteries. Usually, blood flow in arteries is considered to be laminar, but in case of stenosis turbulent regime can appear in post-stenotic region as a result of narrowing caused by plaque formation (Fig. 3).

Figure 3. Flow regimes in blood vessel

FFR_{CT} computation combining coronary computed tomographic (CT) angiography and CFD simulations has been validated in a few multicenter clinical trials (DISCOVER-FLOW, DeFACTO, NXT) as a non-invasive technique for assessing functional significance of stenosis. The most essential steps in this technique are [14, 21]: (i) creation of the computational domain (3D coronary anatomic model) using images obtained from coronary CT, (ii) prescription of inlet and outlet haemodynamic boundary conditions and (iii) application of CFD numerical method to solve the governing equations.

Computational Fluid Dynamics (CFD) represents an efficient tool for solving the governing equations of fluid flow. The conversion of those partial different equations into a system of algebraic equations can be performed by using different methods, such as finite element or finite volume methods [28].

To perform a CFD simulation of coronary artery flow three-dimensional atomic model is needed. There are several techniques that have been applied to provide it. The most common are based on biplane coronary angiography and rotational coronary angiography.

Boundary conditions have to be imposed at the inlet and outlet of the computational domain. Classical inlet boundary conditions are pressure or flow. Inlet pressure can be taken from patient-specific measurement, but also from population average data. Flow rate can be extracted from imaging modalities [29]. At the outlet section boundary conditions are usually derived by fixing flow rate [30]. At wall boundary no-slip condition is applied.

After generating the computational domain and imposing the appropriate boundary conditions CFD method computes the pressure and velocity fields. From these values the FFR_{CT} is obtained in each domain point by normalizing the average coronary artery pressure field by the average aortic pressure during the period of maximum hyperaemia. This enables calculation of FFR_{CT} in the whole computational (vascular) domain, thus, across stenotic region as well. The Navier-Stokes equations may be solved by using many deferent solvers, such as ANSYS Fluent, CFD module, PAK, Star-CCM+, PAKF, OpenFOAM, etc. Of note, it has been shown that FFR_{CT} has an uncertain zone between the values of 0.75 and 0.80 [31]. In that range a lower accuracy has been observed. On the other hand, it has been proven that the values $FFR_{CT} > 0.90$ and $FFR_{CT} \leq 0.60$ provide much greater certainty.

In general, the approach based on CFD technique involves different algorithms which can be based on full or reduced-order CFD modelling. Although full order CFD approach has shown promising results when compared to invasive FFR measurements, yet it is pretty time-consuming procedure which requires high performance computers [24]. In order to overcome these limitations, the reduced-order models have been introduced. Reduced-order models (1D and 2D models) still provide satisfactory accuracy with significantly shorter computational time.

Typical 1D model considers only an axial dimension along the centreline of the blood vessel. The Navier-Stokes equations are integrated over the cross-section while assuming an

axisymmetric parabolic cross-sectional velocity profile [32]. Due to the lack of full spatial information 1D models can only compute an average axial velocity and pressure gradients.

Two-dimensional (2D) methods do not require a cross-sectional velocity profile to be prescribed and have the ability to capture flow separation. Ghigo et al. [33] proposed 2D model which divides the cross section of blood vessel into a number of coaxial rings. The Navier-Stokes equations are integrated assuming a constant axial velocity over each ring. Consequently, the cross-sectional profile of the axial velocity is calculated instead of being assumed. This also means different velocity profiles along the axial coordinate providing detection of potential flow separation.

Various analytical models have been developed to compute the pressure drop along lesions needed for calculation of FFR. All these models are similar and represent generalization of Bernoulli's equation (law of conservation of energy) [34-37]. The common for most of these models is that they treat a stenosis as a local fluid resistance where a sudden pressure drop appears. Assuming an incompressible flow, the pressure drop (eq. 6) can be expressed in terms of volumetric flow rate and have the following general form [38]:

$$\Delta P = k_1 Q + k_2 Q^2 + k_3 \frac{\partial Q}{\partial t}. \tag{7}$$

where Δp represents the pressure drop and k_1, k_2 and k_3 are coefficients, not known a priori, but should be modelled. Three terms on the right-hand side represents viscous, turbulent, and inertial pressure drops. The first term refers to laminar flow where the pressure drop linearly depends on the flow rate. The quadratic term takes into account the pressure drop caused by the turbulence downstream of stenosis and flow separation [39]. Young et al [40] developed their model relying on equation (7), thus, taking into account three types of pressure losses.

Seeley and Young [35] use the similar approach:

$$\Delta P = \frac{\mu K_v}{2\pi R_0^3} Q + \frac{\rho K_t}{2A_0^2}\left(\frac{A_0}{A_s}-1\right)^2 Q|Q| + \frac{\rho K_u L_s}{A_0}\frac{\partial Q}{\partial t},\tag{8}$$

where

$$K_v = \frac{32L_a}{D_0}\left(\frac{A_0}{A_s}\right)^2, \quad L_a = 0.83L_s + 1.64D_s, \quad K_t = 1.52, \quad K_u = 1.2.$$

D_0 and D_s are the cross-sectional diameters of native vessels and stenosis, respectively; L_S is the length of the stenosis, K_v is the viscosity coefficient, K_t is the turbulence coefficient and K_u is the inertial coefficient.

Garcia et al [34] calculate the pressure drop using the following expression:

$$\Delta P = \frac{\rho Q^2}{2}\left(\frac{1}{A_s^2}-\frac{1}{A_0^2}\right) + \frac{\rho\alpha}{\sqrt{A_0}}\left(\frac{A_0}{A_s}-1\right)^\beta \frac{\partial Q}{\partial t},\tag{9}$$

where Q represents the flow rate, A_s is minimal cross-section of the stenosis, A_0 is the nominal cross-section of the native vessel, and $\alpha = 6.28$ and $\beta = 0.5$ are empirically derived parameters.

Itu et al. [36] calculate the pressure drop as follows:

$$\Delta P = K_v(\alpha)R_{vc}Q + \frac{\rho K_t}{2A_0^2}\left(\frac{A_0}{A_s}-1\right)^2 Q|Q| + K_u L_u \frac{\partial Q}{\partial t} + K_c(\alpha)R_{vc}\bar{Q},\tag{10}$$

where

$$K_v = 1 + 0.053\left(\frac{A_s}{A_0}\right)\alpha^2, \quad K_c = 0.0018\alpha^2, \quad K_t = 1.52, \quad K_u = 1.2.$$

$$R_{vc} = \frac{8\mu}{\pi}\int_0^{L_s}\frac{1}{R(x)^4}\,dl, \quad L_u = \frac{\rho}{\pi}\int_0^{L_s}\frac{1}{R(x)^2}\,dl, \quad \alpha = R_0\sqrt{\frac{\rho f}{\mu}}, \quad f = HR\left(\frac{2\pi}{60}\right)$$

This model is similar to the model proposed by Seeley and Young, however, the viscous resistance R_{vc} (in the first term) is here calculated by using Poiseuille's law. The second and the third terms represent the turbulent and inertial losses, respectively. The fourth term models the phase difference between flow rate and pressure drop. L_u is the inertance, $\bar{Q}$ is the mean flow rate, while K_c represents a continuous coefficient with α being the Womersley number.

In case of a steady flow the third term is omitted. Papafaklis et al. [41] linked pressure drops to flow using only two first terms:

$$\Delta P = f_v Q + f_s Q^2 , \tag{11}$$

where fv is the coefficient of pressure loss due to viscous friction, and fs is the coefficient of pressure loss due to turbulence.

The unknown coefficients f_v and f_s can be determined from equation (11) by using two values for pressure drop. Equation (11) can be rewritten as follows:

$$\frac{P_d}{P_a} = 1 - f_v \frac{Q}{P_a} + f_s \frac{Q^2}{P_a} \tag{12}$$

The area under the curve P_d/P_a vs. Q is then calculated for a flow range between 0 and 4 ml/s (mean+2SD increase of the hyperemic flow rate in a normal human coronary artery). After that, nFFR is calculated for each case as the ratio of the area under the artery-specific P_d/P_a vs. Q curve to the reference area.

Huo et al. [42], however, introduced an analytical model without empirical parameters. Their model also originates from Bernoulli's equation and takes into account different pressure losses along stenosis. The input variables are hyperaemic flow rate, the length of the lesion, as well as the proximal, distal and minimal cross-sectional areas along the lesion.

3. The methods for Fractional flow reserve (FFR) determination

Here, we present the modelling of coronary artery blood flow and pressure drop in human coronary arteries using image-based CFD and analytical models. Later, these results are compared to the experimental ones obtained clinically by means of pressure wire.

3.1 Numerical method

The determination of flow and pressure field in a stenosed coronary artery, which is necessary to calculate Numerical Fractional Flow Reserve (nFFR), is here performed by employing the governing equations of fluid dynamics which relate to momentum (Navier-Stokes equations) and mass (the continuity equation) conservation [43]:

$$\rho\left(u_i \cdot \nabla\right)u_i + \nabla p_i - \mu\Delta u_i = 0, \tag{13}$$

$$\nabla u_i = 0. \tag{14}$$

where u_i is velocity, p_i is pressure, μ is dynamic viscosity and ρ is density of blood (∇ is the Hamiltonian, $\Delta \equiv \nabla^2$ is Laplacian). The fluid is assumed to be steady, incompressible and laminar, while the external body force is neglected.

To determine blood flow and pressure fields in coronary arteries the computational domain has to be designed and boundary conditions need to be specified. Three-dimensional arterial anatomy is generated using a medical 3D image-processing engineering software *Mimics*. This software creates 3D surface models from Computed Tomography (CT) stacks of 2D image data. For further transformation of 3D scans of physical object into parametric models the complete toolbox *Geomagic Studio* is applied. After the reconstruction of the anatomical surface, a mesh is generated using **FEMAP** (Finite Element Modelling and Post-processing)

engineering analysis program. A linear tetrahedron is used as the final element. **FEM_PAK** (in-house developed) is further used in order to insert initial parameters and input functions for converting tetrahedron element into hexahedron element which are more computationally efficient in this type of simulation. Numerical simulation, based on finite element method, is performed by using **PAKF solver** [44]. And, finally, for visualization of the results obtained **CAD** post-processing software is applied.

In this case, blood flow through the right coronary arteries (RCA) was simulated. Blood was considered as an incompressible Newtonian fluid with a dynamic viscosity of $\mu = 0.00365$ Pas and density of $\rho = 1050$ kg/m^3. In order to calculate the nFFR value two separate simulations are performed for each case, applying a pressure of 100 mmHg at the inlet and flow rates of 1 and 3 ml/s at the outlet.

3.2 Analytical method

In this paper the pressure drop calculation is based on the analytical model [42] with no empirical parameters. This model is derived from energy conservation which takes into account various pressure losses:

$$\Delta P = \Delta P_{conv} + \Delta P_{const} + \Delta P_{diff} + \Delta P_{exp}, \tag{15}$$

where ΔP_{conv}, ΔP_{const}, ΔP_{dif} and ΔP_{exp} are pressure drops due to flow convection, sudden constriction in cross-sectional area from proximal normal vessel to stenosis, flow diffusion and sudden expansion in cross-sectional area from stenosis to distal normal vessel, respectively.

Pressure drop due to flow convection is:

$$\Delta P_{conv} = \frac{\rho}{2}\left(V_{out}^2 - V_{in}^2\right) = \frac{\rho Q^2}{2}\left(\frac{1}{A_{out}^2} - \frac{1}{A_{in}^2}\right), \tag{16}$$

where ρ is blood density, V is velocity, Q is the hyperaemic flow rate, while A_{in} and A_{out} are the cross-sections at inlet and outlet.

In case the flow transition from proximal vessel to stenosis is relatively smooth, the pressure (energy) loss due to a sudden constriction can be neglected, thus,

$$\Delta P_{const} = 0. \tag{17}$$

The pressure drops due to flow diffusion ΔP_{dif} is caused by viscosity and it causes an acceleration of the flow. It can be supposed that in the entrance region of stenosis there exists an inviscid core, with a dimensionless radius (φ), in which the velocity is uniform [43]. At the inlet φ = 1, between the inlet and the fully developed region 0 < φ < 1, while at the fully developed region φ = 0. The non-dimensional radius of inviscid core (φ) is calculated from the following expression [42]:

$$\frac{\pi\mu L_{sten}}{4\rho Q} = \frac{1}{4}\int_{\varphi}^{1}\frac{(1-\varphi)(6+\varphi)\left(1+4\varphi+9\varphi^2+4\varphi^3\right)}{5\varphi(3+2\varphi)\left(3+2\varphi+\varphi^2\right)^2}d\varphi. \tag{18}$$

In case φ < 0.05, that is most common for coronary artery ΔP_{dif} and ΔP_{exp} are:

$$\Delta P_{diff} = \frac{\rho Q^2}{2A_s^2}\frac{96}{5}\int_{\varphi}^{1}\frac{\left(1+4\varphi+9\varphi^2+4\varphi^3\right)}{\varphi(3+2\varphi)\left(3+2\varphi+\varphi^2\right)^2}d\varphi + 8\pi\mu Q\int_{0}^{L_v-L_s}\frac{1}{A(x)^2}dx \tag{19}$$

$$\Delta P_{exp} = \frac{\rho Q^2}{2}\left(\frac{1}{A_s}-\frac{1}{A_{in}}\right)^2 + \left[2\left(\frac{1}{A_s}-\frac{1}{A_{in}}\right)\left(\frac{1}{A_s}-\frac{1}{3}\frac{1}{A_{in}}\right)-\left(\frac{1}{A_s}-\frac{1}{A_{in}}\right)^2(1-\varphi)^2\right] \tag{20}$$

The total pressure drop is

$$\Delta P = \frac{\rho}{2}\left(V_{out}^2 - V_{in}^2\right) = \frac{\rho Q^2}{2}\left(\frac{1}{A_{out}^2} - \frac{1}{A_{in}^2}\right) + \frac{\rho Q^2}{2A_s^2}\frac{96}{5}\int_\varphi^1 \frac{\left(1 + 4\varphi + 9\varphi^2 + 4\varphi^3\right)}{\varphi\left(3 + 2\varphi\right)\left(3 + 2\varphi + \varphi^2\right)^2}\,d\varphi +$$

$$+ 8\pi\mu Q \int_0^{L_v - L_s} \frac{1}{A(x)^2}\,dx + \frac{\rho Q^2}{2}\left(\frac{1}{A_s} - \frac{1}{A_{in}}\right)^2 + \tag{21}$$

$$+ \left[2\left(\frac{1}{A_s} - \frac{1}{A_{in}}\right)\left(\frac{1}{A_s} - \frac{1}{3}\frac{1}{A_{in}}\right) - \left(\frac{1}{A_s} - \frac{1}{A_{in}}\right)^2 \left(1 - \varphi\right)^2\right]$$

All needed artery dimensions (diameters, lengths, areas) are used to calculate ΔP value (eq. 21). Then, using equations 11 and 12 previously unknown parameters (f_v and f_s) are calculated and aFFR is defined.

4. Results and discussion

The values for FFR are computed for twenty patients using numerical method (CFD and CCTA), as well as using simplified analytical method based on Bernoulli's law. These results are compared with the clinical data for FFR obtained by using a flow-pressure wire under the induction of hyperemia (Table 1).

Table 1

FFR values (numerical, analytical and clinical data) for 20 patients

Figure 4 shows the result for three patients after numerical simulation in case of flow rate of 3 ml/s. A black circle can be seen on the picture, which marks the observed stenosis on the artery. The medically measured FFR, if compared to the analytical one, for this patient's case, differs by about 4%, while if compared to the numerical FFR, the difference is about 2.6%.

Figure 4. Pressure distribution in right coronary artery (for the patients No 10, 2 and 19)

Figures 5 and 6 shows the coefficient of determination between the observed FFR values. It can be seen that the coefficient of determination has a very good correlation with a value of 0.91 (Fig. 5), when comparing medical and numerical FFR.

Figure 5. Coefficient of determination between medical and numerical FFR.

A slightly lower value of 0.81 is observed between medical and analytical FFR (Fig. 6).

Figure 6. Coefficient of determination between medical and analytical FFR.

As known, an FFR lower than 0.75-0.80 is generally considered to be associated with myocardial ischemia. If FFR values below 0.8 are extracted from Table 1 and the differences are analyzed, the following was obtained: the standard error has a value 0.01201, while the standard deviation was 0.02081. When considering FFR values above 0.80, it is found that the standard error was 0.01527, and the standard deviation was 0.02645. It can be concluded, based on the medical, numerical and analytical FFR values of twenty coronary geometries, that the standard deviation is higher for FFR values above 0.80, as well as the standard error. There was a good agreement between the two parameters medically measurement and numerical FFR by Bland-Altman method of analysis (Figure 7). The mean difference of measurements from the two methods was 0.02 (SD=0.0292, $p<0.0001$), indicating a small systematic overestimation of the medical FFR by numerical FFR. Corresponding limits of agreement were from -0.02935 to 0.077232.

Figure 7. Bland-Altman plot between nFFR and mFFR.

Limitation of the study

Limitation of this study is total number of 20 patients. Further research could go in direction of providing more patients and more precise localization of the stenosis. That means statistical analysis of the hemodynamically significant lesions or not.

5. Conclusion

This study has validated the analytical model and reliability of simulations for calculation of FFR values. As it was presented, analytical model originates from Bernoulli's equation and takes into account different pressure losses along stenosis. Those two methods were validated for twenty models of coronary arteries. The non-invasive measurements of FFR are promising tool for the assessment of the hemodynamic significance of intermediate coronary arteries stenosis. The procedure presented in the paper is useful because theoretical knowledge is applied directly to real problems (patients). The values of the pressure change are calculated and fractional flow reserve indexes are determined. The required analysis time was less then hour and that was significantly lower when compared to the most known FFR method. This approach to assessing the condition of the coronary artery is more favorable due to the fact that it is a non-invasive technique. Definitely, FFR gives the answer to the question of whether patients need a stent, bypass surgery or are treated only with drugs.

Our Bland-Altman analysis have been shown that the mean difference of measurements from the medical measurement and numerical FFR was 0.02 (SD=0.0292, p<0.0001) which is in good agreement.

Conflict of interest

The authors declare that they have no conflict of interest.

REFERENCES

[1]   Townsend N, Wilson L, Bhatnagar P, Wickramasinghe K, Rayner M, Nichols M. Cardiovascular disease in Europe: epidemiological update 2016. European Heart Journal. 2016; 37: 3232-3245.

[2]   Roger VL, Go AS, Lloyd-Jones DM, Adams RJ, Berry JD, Brown TM, et al. Heart disease and stroke statistics-2011 update: A report from the American Heart Association. Circulation. 2011; 123: e18–e209.

[3]   Fihn SD, Blankenship JC, Alexander KP, Bittl J A, Byrne JG, Fletcher BJ, et al. 2014 ACC/AHA/AATS/ PCNA/SCAI/STS focused update of the guideline for the diagnosis and management of patients with stable ischemic heart disease. Circulation. 2014; 130: 1749-1767.

[4]   Demir O, Rahman H, P van de Hoef T, Escaned J, Piek JJ, Plein S, Perera D. Invasive and non-invasive assessment of ischaemia in chronic coronary syndromes: translating pathophysiology to clinical practice. European Heart Journal. 2022; 43(2): 105-117.

[5]   Bhatt, DL. Fractional Flow Reserve Measurement for the Physiological Assessment of Coronary Artery Stenosis Severity. JAMA. 2018; 320(12): 1275-1276.

[6]   Mowatt G, et al. Systematic review of the clinical effectiveness and cost-effectiveness of 64-slice or higher computed tomography angiography as an alternative to invasive angiography in the investigation of coronary artery disease. Health Technol Assess. 2008; 12:17.

[7]   Min JK, Shaw LJ, Berman DS. The present state of coronary computed tomography angiography a process in evolution. Journal of the American College of Cardiology. 2010; 55(10): 957-965.

[8]   Hoffmann MH, Shi H, Schmitz BL, et al. Noninvasive coronary angiography with multislice computed tomography. JAMA 2005; 293(20): 2471-2478.

[9]   Meijboom WB, Meijs MF, Schuijf JD, et al. Diagnostic accuracy of 64-slice computed tomography coronary angiography: a prospective, multicenter, multivendor study. Journal of the American College of Cardiology. 2008; 52(25): 2135-2144.

[10]   Dewey M. Coronary CT versus MR angiography: pro CT—the role of CT angiography. Radiology 2011; 258(2): 329-339.

[11]   Secchi F, Alı M, Faggiano E, Cannao PM, Fedele M, Tresoldi S, Di Leo G, Auricchio F, Sardanelli F. Fractional flow reserve based on computed tomography: an overview. European Heart Journal Supplements. 2016; 18 (Supplement E), E49-E56.

[12]   De Bruyne B, Pijls NH, Kalesan B, et al. Fractional flow reserve-guided PCI versus medical therapy in stable coronary disease. New England Journal of Medicine. 2012; 367(11): 991-1001.

[13]   Min JK, Leipsic J, Pencina MJ, et al. Diagnostic accuracy of fractional flow reserve from anatomic CT angiography. JAMA. 2012; 308: 1237-1245.

[14]   Tesche C, De Cecco CN, Albrecht MH, Duguay TM, Bayer RR, Litwin SE, et al. Coronary CT angiography-derived fractional flow reserve. Radiology. 2017; 285(1): 17-33.

[15]   Tonino PAL, De Bruyne B, Pijls NHJ, et al. Fractional flow reserve versus angiography for guiding PCI in patients with multivessel coronary disease (FAME study). New England Journal of Medicine. 2009; 360: 213-24.

[16]   Coenen A et al. Fractional Flow Reserve Computed from Noninvasive CT Angiography Data: Diagnostic Performance of an On-Site Clinician-operated Computional Fluid Dynamics Algorithm. Radiology. 2015; 274(3): 674-683.

[17]   Pijls NH, De Bruyne B, Peels K, et al. Measurement of fractional flow reserve to assess the functional severity of coronaryartery stenoses. New England Journal of Medicine. 1996; 334: 1703-8.

[18]   Spaan JAE, Piek JJ, Hoffman JIE, Siebes M. Physiological Basis of Clinically Used Coronary Hemodynamic Indices. Circulation. 2006; 113: 446-455.

[19]   Hakeem A, Mouhamad A, Leesar MA. Fractional flow reserve: a new paradigm for diagnosis and management of coronary artery disease. Interv. Cardiology. 2012; 4(1): 61-71.

[20]   Molloi S, Zhou Y, Kassab GS. Regional volumetric coronary blood flow measurement by digital angiography: in vivo validation. *Acad Radiol.* 2004; 11: 757-766.

[21]   Wong JT, Le H, Suh WM, Chalyan DA, Toufan Mehraien T, Kern MJ, Kassab GS, Molloi S. Quantification of fractional flow reserve based on angiographic image data. The International Journal of Cardiovascular Imaging. 2012; 28(1): 13-22.

[22]   Zhang Z, Takarada S, Molloi S. Assessment of coronary microcirculation in a swine animal model. American Journal of Physiology-Heart and CirculatoryPhysiology. 2011; 301(2): H402-408.

[23]   Faes TJC, Meer R, Heyndrickx GR and Kerkhof PLM. Fractional Flow Reserve Evaluated as Metric of Coronary Stenosis - A Mathematical Model Study. Front. Cardiovasc. Med. 2020; (6): 189

[24]   Taylor CA, Fonte TA, Min JK. Computational fluid dynamics applied to cardiac computed tomography for noninvasive quantification of fractional flow reserve: Scientific basis. J Am Coll Cardiol. 2013; 61: 2233–2241.

[25] Kim HJ, Vignon-Clementel IE, Figueroa CA, Ladisa JF, Jansen KE, Feinstein JA TC. On coupling a lumped parameter heart model and a three-dimensional finite element aorta model. Ann Biomed Eng. 2009; 37: 2153–2169.

[26] Min JK, Leipsic J, Pencina MJ et al. Diagnostic accuracy of fractional flow reserve from anatomic CT angiography. JAMA 2012; 308(12), 1237–1245.

[27] Pantos I, Katritsis D. Fractional Flow Reserve Derived from Coronary Imaging and Computational Fluid Dynamics. Interv Cardiol. 2014; 9(3): 145-150.

[28] Tu J, Yeoh GH, Liu C. Computational Fluid Dynamics: A Practical Approach, Butterworth-Heinemann, 2018. 601 p. ISBN 978-0-08-101127-0.

[29] Yu W, Huang J, Jia D, Chen S, Raffel OC, Ding D, Tian F, Kan J, Zhang S, Yan F, Chen Y, Bezerra HG, Wijns W, Tu S. Diagnostic accuracy of intracoronary optical coherence tomography-derived fractional flow reserve for assessment of coronary stenosis severity. EuroIntervention 2019; 15: 189–197

[30] Razavi A, Sachdeva S, Frommelt PC, LaDisa JF. Computational Assessment of Hemodynamic Significance in Patients With Intramural Anomalous Aortic Origin of the Coronary Artery Using Virtually Derived Fractional Flow Reserve and Downstream Microvascular Resistance. J Biomech Eng. 2022; 144: 031005.

[31] De Bruyne B, Sarma J. Fractional flow reserve: a review: invasive imaging. Heart. 2008; 94: 949–59. doi: 10.1136/hrt.2007.122838

[32] Bessems D. On the propagation of pressure and flow waves through the patient-specific arterial system. Ph.D. Thesis, TU Eindhoven, The Netherlands, 2007.

[33] Ghigo, A. R., Fullana, J. M., and Lagrée, P. Y. A 2D Nonlinear Multi-ring Model for Blood Flow in Large Elastic Arteries, J. Comput. Phys. 2017; 350: 136–165.

[34] Garcia, D. , Pibarot, P. , and Duranda, L. G. Analytical Modeling of the Instantaneous Pressure Gradient Across the Aortic Valve, J. Biomech. 2005; 38(6): 1303–1311.

[35]   Seeley, B. D., and Young, D. F. Effect of Geometry on Pressure Losses Across Models of Arterial Stenosis, J. Biomech. 1976; 9(7): 439–448.

[36]   Itu L, Sharma P, Ralovich K, Mihalef V, Ionasec R, Everett A, et al. Non-invasive hemodynamic assessment of aortic coarctation: validation with in vivo measurements. Ann. Biomed. Eng. 2013; 41(4): 669–681.

[37]   Mirramezani M, Diamond S, Litt H, Shadden SC. Reduced order models for transstenotic pressure drop in the coronary arteries. J Biomech Eng. 2019; 141(3): 0310051-03100511

[38]   Lyras KG, Lee J. An improved reduced-order model for pressure drop across arterial stenosis. PLoS One. 2021; 16 (10): e0258047.

[39]   Gould KL. Pressure-flow characteristics of coronary stenoses in unsedated dogs at rest and during coronary vasodilation. Circulation research. 1978; 43(2): 242–253.

[40]   Young DF, Cholvin NR, Kirkeeide RL, Roth AC. Hemodynamics of arterial stenoses at elevated flow rates. Circulation Research. 1977; 41(1): 99–107.

[41]   M. I. Papafaklis, T. Muramatsu, Y. Ishibashi et al., Fast virtual functional assessment of intermediate coronary lesions using routine angiographic data and blood flow simulation in humans: comparison with pressure wire - fractional flow reserve, Euro Intervention. 2014; 10(5): 574–583.

[42]   Huo Y, Svenson M, Choy JS, Zhang ZD, Kassab GS. A validated predictive model of coronary fractional flow reserve Journal of the Royal Society Interface. 2012; 9: 1325-1338.

[43]   Saha S, Purushotham T, Prakash KA. Numerical and experimental investigations of Fractional Flow Reserve (FFR) in a stenosed coronary artery. E3S Web of Conferences ICCHMT 2019.

[44]   Kojić M, Filipović N, Slavković R, Živković M, Grujović N. PAKF: Program for FE analysis of fluid flow with heat transfer, Faculty of Mechanical Engineering University of Kragujevac, 1998.

Normal Artery   Narrowing of Artery

Lipid deposit of
plaque
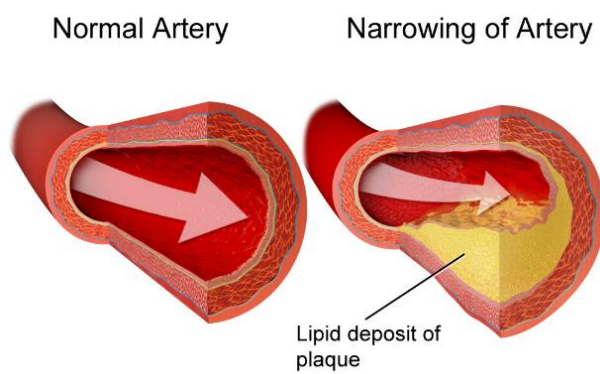
Figure 1. Coronary artery disease [2]
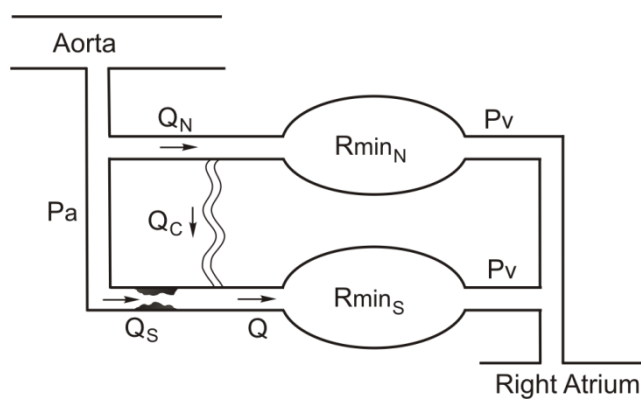
Figure 2. Model of the coronary circulation
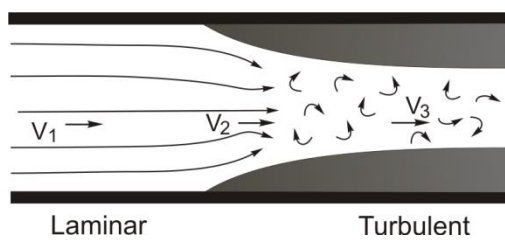
Figure 3. Flow regimes in blood vessel
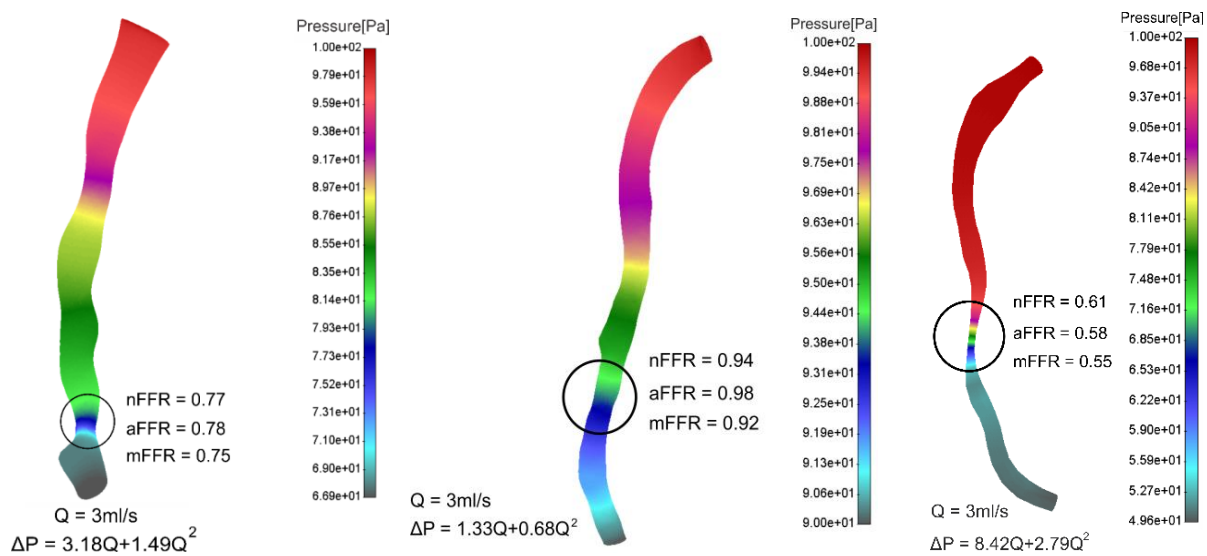
Figure 4. Pressure distribution in right coronary artery (for the patients No 10, 2 and 19)
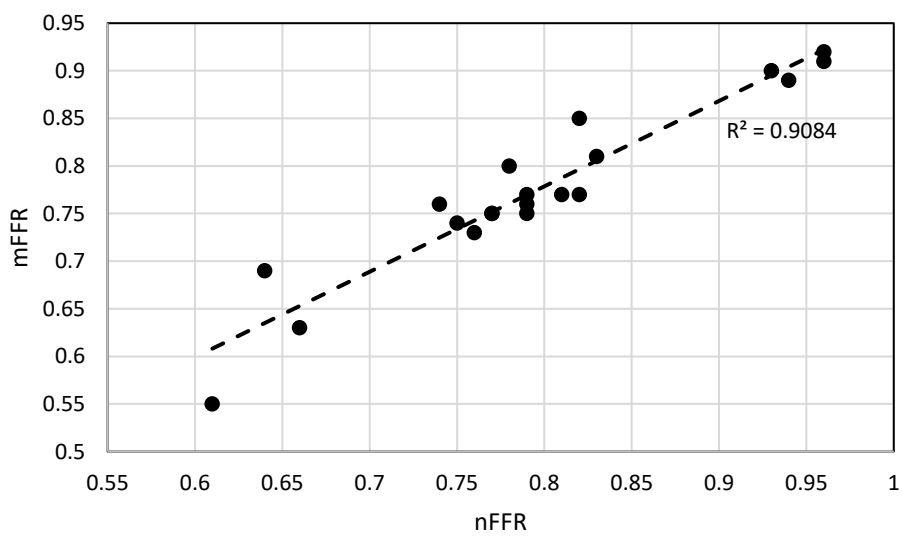
Figure 5. Coefficient of determination between medical and numerical FFR.
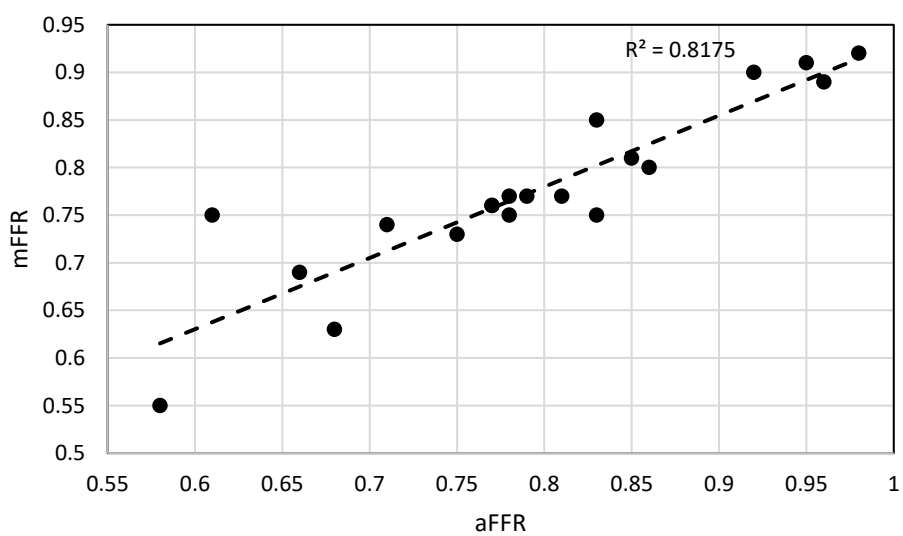
Figure 6. Coefficient of determination between medical and analytical FFR.
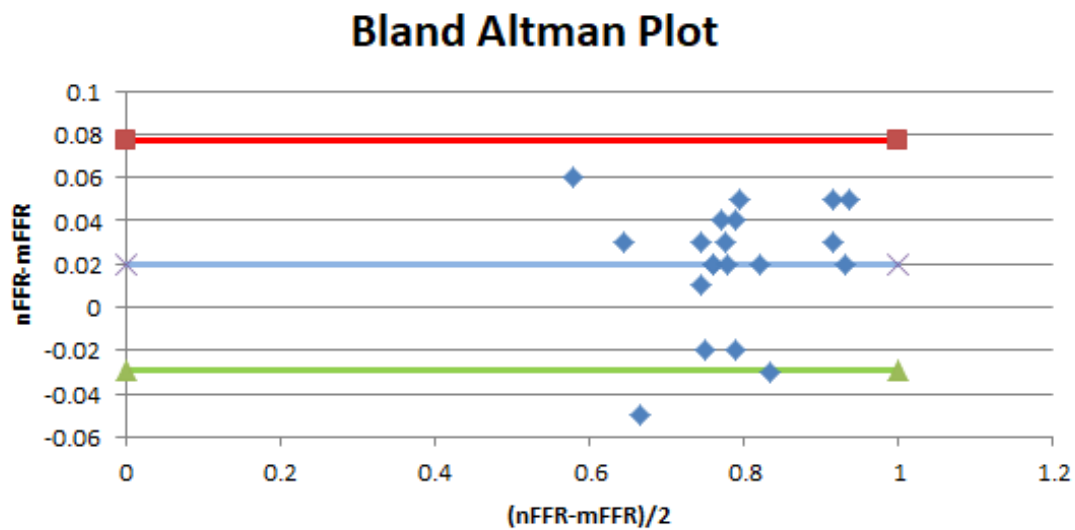
Figure 7. Bland-Altman plot between nFFR and mFFR.

Table 1

FFR values (numerical, analytical and clinical data) for 20 patients

	nFFR*	aFFR*	mFFR*
Pat. 1	0.94	0.96	0.89
Pat. 2	0.94	0.98	0.92
Pat. 3	0.78	0.86	0.80
Pat. 4	0.77	0.61	0.75
Pat. 5	0.93	0.92	0.90
Pat. 6	0.96	0.95	0.91
Pat. 7	0.82	0.83	0.85
Pat. 8	0.74	0.77	0.76
Pat. 9	0.81	0.79	0.77
Pat. 10	0.77	0.78	0.75
Pat. 11	0.79	0.81	0.77
Pat. 12	0.76	0.75	0.73
Pat. 13	0.75	0.71	0.74
Pat. 14	0.66	0.68	0.63
Pat. 15	0.82	0.78	0.77
Pat. 16	0.79	0.83	0.75
Pat. 17	0.83	0.85	0.81
Pat. 18	0.79	0.77	0.76
Pat. 19	0.61	0.58	0.55
Pat. 20	0.64	0.66	0.69

*aFFR – analytical FFR; nFFR – numerical FFR; mFFR – medical FFR